nature photonics

SUPPLEMENTARY INFORMATION

https://doi.org/10.1038/s41566-018-0156-x

In the format provided by the authors and unedited.

Enrichment of molecular antenna triplets amplifies upconverting nanoparticle emission

David J. Garfield[1,2,8], Nicholas J. Borys[1,8], Samia M. Hamed[2], Nicole A. Torquato[1], Cheryl A. Tajon[1], Bining Tian[1], Brian Shevitski[1,3], Edward S. Barnard[1], Yung Doug Suh[4,5], Shaul Aloni[1], Jeffrey B. Neaton[1,3,6], Emory M. Chan[1]*, Bruce E. Cohen[1]* and P. James Schuck[1,7]*

[1]The Molecular Foundry, Lawrence Berkeley National Laboratory, Berkeley, CA, USA. [2]Department of Chemistry, University of California, Berkeley, CA, USA. [3]Department of Physics, University of California, Berkeley, CA, USA. [4]Research Center for Convergence NanoRaman Technology, Korea Research Institute of Chemical Technology, DaeJeon, South Korea. [5]School of Chemical Engineering, Sung Kyun Kwan University (SKKU), Suwon, Korea. [6]Kavli Energy NanoSciences Institute at Berkeley, Berkeley, CA, USA. [7]Department of Mechanical Engineering, Columbia University, New York, NY, USA. [8]These authors contributed equally: David J. Garfield, Nicholas J. Borys. *e-mail: emchan@lbl.gov; becohen@lbl.gov; p.j.schuck@columbia.edu

Supplementary Materials for

Enrichment of molecular antenna triplets amplifies upconverting nanoparticle emission

David J. Garfield[†], Nicholas J. Borys[†], Samia M. Hamed, Nicole A. Torquato, Cheryl A. Tajon, Bining Tian, Brian Shevitski, Edward S. Barnard, Yung Doug Suh, Shaul Aloni, Jeffrey B. Neaton, Emory M. Chan[*], Bruce E. Cohen[*], P. James Schuck[*]

*Corresponding authors. email: p.j.schuck@columbia.edu, emchan@lbl.gov, becohen@lbl.gov

This PDF file includes:

Supplementary Methods

Materials

Sodium oleate, ammonium fluoride (anhydrous), oleic acid (OA, 90%), 1-octadecene (ODE, 90%), IR780 iodide, 4-mercaptobenzoic acid, poly(methyl methacrylate) (PMMA), cyclooctatetraene (COT), chloroform, hexanes, acetonitrile, dimethylformamide (DMF), trimethylamine (Et3N), anhydrous ethanol (EtOH) and toluene were purchased from Sigma. Anhydrous lanthanide trichlorides were purchased from Strem.

Flask Synthesis of Core UCNPs

UCNPs were synthesized using air-free Schlenk techniques as reported previously[1] with some modifications. For $NaY_{0.48}Gd_{0.3}Yb_{0.2}Er_{0.02}F_4$ UCNPs: to a dry 50-mL 3-neck flask, YCl_3 (192 μmol, 37.5 mg), $YbCl_3$ (80 μmol, 22 mg), $ErCl_3$ (8 μmol, 2.2 mg), and $GdCl_3$ (120 μmol, 32 mg) were added, followed by OA (3.25 g, 11.5 mmol) and ODE (4 mL). The flask was stirred, placed under vacuum and heated to 110 °C for 1 h, causing the solution to become clear. The flask was cooled and filled with N_2, and sodium oleate (1.25 mmol, 381 mg) and NH_4F (2 mmol, 74 mg) were added. The flask was again placed under vacuum and stirred at room temperature for 20 min, and then flushed 3 times with N_2. The reaction was heated to 315 °C, stirred for 45 min under N_2, and then cooled rapidly by a strong stream of air to the outside of the flask following removal of the heating mantle. When the reaction had cooled to 75 °C, EtOH (20 mL) and acetone (20 mL) were added to precipitate the nanocrystals. The reaction was transferred to a centrifuge tube and centrifuged at 3000 × *g* for 5 min to precipitate the nanocrystals completely. The supernatant was discarded and the white solid (~80 mg) was resuspended in minimal hexanes (5 mL) to break up the pellet. The nanocrystals where then precipitated again with addition of EtOH (45 mL) and centrifuged at 3000 × *g* for 5min. The nanocrystals were resuspended and stored in 10 mL of hexanes with 0.2% (*v/v*) oleic acid to give a ~10 mM dispersion.

Because added Gd^{3+} typically yields smaller nanocrystals[2], UCNPs with 30% Gd^{3+} content were grown at 320 °C.

Automated Synthesis of UCNPs

The Workstation for Automated Nanomaterial Discovery and Analysis (WANDA) robot was sometimes used to explore the synthesis space[1]. When WANDA was used, the High-throughput Experimentation Robot for the Multiplexed Automation of Nanochemistry (HERMAN) robot was used to dispense solid materials. For $NaY_{0.48}Gd_{0.2}Yb_{0.2}Er_{0.02}F_4$ UCNPS: a precursor solution of Ln-oleate was prepared by adding YCl_3 (3.51 mmol, 685 mg), $YbCl_3$ (0.90 mmol, 252 mg), and $ErCl_3$ (0.090 mmol, 25 mg) to a 100 mL round-bottom flask. OA (24.4 g) and ODE (14.2 g) were added, and the solution was heated to 110 °C under vacuum while stirring, and held at this temperature for 1 h to form a homogenous clear solution. The solution was then cooled to room temperature and brought under vacuum into an N_2 glovebox equipped with the WANDA robot. To each reaction vial were added solid sodium oleate (1.25 mmol, 380 mg) and NH_4F (2 mmol, 74 mg), using the HERMAN robot. This was followed by the Ln-oleate solution (4.38 g) and additional ODE (such that the total mass of ODE = 5.5 g). The reaction vials were heated using the WANDA reactor at 30 °C/min to temperatures

of 280 – 330 °C and held at that temperature for 30-90 min. The reactors were cooled to 75 °C, after which 9 mL of EtOH was added to precipitate the nanoparticles. Cleaning was then performed analogously to flask synthesis.

Synthesis of Core/Shell UCNPs

$NaYF_4$ or $NaGdF_4$ shells were grown using a protocol adapted from Li *et al.*[3] Briefly, UCNP cores in hexanes were dried in a three-neck 50 mL round bottom flask using gentle N_2 flow. Dry UCNPs were dispersed in 4 mL of OA and 6 mL of ODE and stirred under vacuum at 70 °C for 1 hour. UCNPs were then heated under N_2 to 280°C. For $NaYF_4$ shells, sequential injections of 0.1 M yttrium oleate dissolved in 40% (*v*/*v*) OA in ODE and 0.4 M sodium trifluoroacetate in OA were performed every 15 min. For $NaGdF_4$ shells, 0.1 M gadolinium oleate dissolved in 40% (*v*/*v*) OA in ODE and 0.4 M sodium trifluoroacetate in OA were utilized. Lanthanide and sodium precursors were added in a 1:2 molar ratio. At the end of an injection series, the reaction mixture was kept at 280°C for 30 min and then cooled with a stream of air until it reached room temperature before cleaning as described above.

Nanoparticle characterization

TEM was performed using a JEOL JEM-2100F field emission transmission electron microscope at an acceleration voltage of 200 kV. Size statistics were acquired for approximately 100 nanoparticles using ImageJ software from multiple High-Angle Annular Dark Field images. X-Ray diffraction (XRD) measurements were performed using a Bruker D8 Discover diffractometer with Cu Kα radiation.

Synthesis of IR806

In a glass vial, IR780 iodide (26 mg, 39 μmol), 4-mercaptobenzoic acid (12 mg, 76 μmol), and Et_3N (12 μL, 86 μmol) were dissolved in 1 mL of dry DMF, and the reaction was stirred at room temperature overnight under N_2. Purification by high-performance liquid chromatography (Varian) on a C_{18} column using a linear gradient of 70 - 100% CH_3CN over 30 minutes gave product eluting at 22 min (84% CH_3CN). NMR (500 MHz, CD_3OD): δ 8.72 (d, 2H, J = 2.8 Hz), 7.91 (d, 2H, J = 1.8 Hz), 7.43-7.24 (m, 10H), 6.32 (d, 2H, J = 3.3 Hz), 4.11 (t, 4H, J = 0.9 Hz), 2.79 (m, 4H), 2.05 (m, 2H), 1.85 (q, 4H, J = 1.1 Hz), 2.15 (s, 12H), 1.02 (t, 6H, J = 1.0 Hz). MS for $C_{43}H_{49}N_2O_2S^+$ calculated: 657.9; found: 658.4.

Functionalization of UCNPs with IR806

IR806 carboxylates are likely to exchange with surface oleates and oleic acids[4] via mass action[5,6], occurring through a two-step X-type ligand exchange, whereby a proton from the substituting ligand is donated to the substituted ligand, which maintains charge neutrality in the nonpolar solvent. Based on reaction stoichiometry, we calculate 40 IR806 molecules per 12-nm UCNP, although their exact distribution on the surface is unknown.

In a typical procedure, 2.7 μL of 7 mM IR806 in $CHCl_3$ was added to an empty vial and the $CHCl_3$ was allowed to evaporate. In a separate microcentrifuge tube, 85 μL of a 5 μM 13-nm UCNP dispersion in toluene were precipitated with excess EtOH and centrifuged. This process was then repeated after resuspension in toluene, and the UCNP

pellet in the microcentrifuge tube, along with the vial containing the dried dye were brought into an N_2 glovebox. The nanoparticle pellet was resuspended in anhydrous toluene, the dye resuspended in anhydrous $CHCl_3$, and the UCNP dispersion added to the vial containing the dye. The mixture was vortexed briefly and kept in the glovebox overnight, and the IR806-UCNP was used without further purification. For variously sized nanoparticles, the total surface area of UCNP was calculated and a surface density of ~1 IR806 molecule per 11 nm^2 was used to functionalize the UCNPs.

IR806-UCNP film encapsulation

After dye-functionalization of the UCNPs, encapsulation was achieved by suspending the IR806-UCNPs in a toluene solution of 5% (*m*/*v*) polystyrene (Sigma) and spin-coating the resulting suspension at 1000 rpm onto a silicon wafer with a 250 nm SiO_x top layer. A ring of UV-curable epoxy resin (Epotek 3035B) was then applied to the film, a glass coverslip pressed onto the ring to form a seal, and the polymer was cured using a UV lamp, with a small piece of foil shading the film to prevent photo-damage from the lamp. This entire procedure was done inside an N_2 glovebox.

Absorption Measurements

All absorption measurements were performed in solution through a quartz cuvette (Starna) using an Agilent Cary Series UV-vis-NIR spectrometer.

Steady-state Fluorescence Measurements

Steady-state fluorescence measurements were primarily obtained with a back-illuminated silicon electron-multiplied CCD chip detector (Andor iXON, model # DU-897E-CSO; QE ~ 17% at 980nm) calibrated with a NIST-certified calibration lamp.

The IR806 emission spectrum in Fig. 2 was obtained with freshly-made ~1 μM solution of HPLC-purified dye (purity >99%, based on liquid chromatography/mass spectrometry), using a Nanolog Spectrofluorometer (Horiba Scientific). These measurements used Xenon lamp excitation at 700 nm and detection using a near-infrared photomultiplier tube with an InP/InGaAs photocathode (Hamamatsu NIR-PMT R5509-73) that was calibrated immediately before these experiments with a NIST-certified calibration lamp (Avantes AvaLight Hal-Cal). This detector operates with a bias voltage of 5V, and has a response range of 300-1700 nm.

Note that the steady-state IR806 singlet emission spectra shown in Fig. 2c are important for guiding understanding and intuition, but that quantification of relative energy transfer is quantified using singlet lifetime data and triplet-quenching measurements. Additionally, the quantification of enhanced emission and quantum yields are measured directly (see, e.g. Fig. 4a and SI Fig. 15).

Spectral Overlap Calculations

The spectral overlap integral, *J*, was calculated for (a) overlap between the normalized dye singlet emission spectrum (area under curve normalized to 1) and the Yb^{3+} molar absorption coefficient (in $M^{-1}\cdot cm^{-1}$); and (b) overlap between the normalized dye triplet spectrum and the Yb^{3+} molar absorption coefficient. For singlet-Yb^{3+} overlap, the *J* value

is 1.40×10^{11} $nm^4 \cdot M^{-1} \cdot cm^{-1}$. In comparison, the triplet-Yb^{3+} overlap *J* value is 3.87×10^{12} $nm^4 \cdot M^{-1} \cdot cm^{-1}$; i.e., *>25 times larger than the singlet-Yb^{3+} overlap*.

Theoretical Calculations

Vertical excitation energies and natural transition orbitals[7] (NTOs) were calculated in Q-Chem utilizing time-dependent density functional theory (TDDFT), the B3LYP exchange-correlation functional, and a VTZ basis set, with solvation effects treated with the ptSS and ptLR polarizable continuum models[8,9]. The lowest lying bright singlet and first triplet transitions are both dominated by π-π* HOMO to LUMO transitions, and the molecule belongs to the cyanine family of dyes whose singlet excitations have been challenging[10,11] to capture with theory. DFT geometry optimization at the B3LYP/VTZ level of theory, performed with two possible initial geometries, yielded two molecular configurations which are pictured below and were of nearly identical energy. The total SCF ground state energy difference at the BHLYP level was 0.08 eV, with the second pictured molecule in the table below having the lower energy. The effect of the choice of the exchange correlation functional (XCF) was explored and, with the Tamm Dancoff approximation (TDA), yielded triplet energies between 0.9 and 1.2 eV. The effect of the TDA was significant in some cases, and its energies are likely more accurate[12]. These results are summarized in Table S1.

Upconverted Emission Measurements

For direct UCNP excitation, a dispersion of UCNPs was added to a sealed quartz cuvette (Starna) and placed on an inverted confocal microscope (Nikon). A 980-nm laser (Thorlabs) is directed into the back aperture of a 0.6 NA 40× Objective (Nikon), and focused through the polished bottom of the cuvette. Emitted light is collected back through the same objective, filtered by two 700-nm short-pass (SP) filters and routed to an LN_2-cooled CCD spectrometer (Princeton Instruments). For dye excitation, an 808 nm laser was used (CrystalLaser). All IR806-UCNP dispersions were handled in an N_2 glovebox from the moment of mixing the dye with the UCNPs through to measurements in the sealed quartz cuvette under N_2. To obtain the power dependence measurements of Figure 4, a continuously variable neutral density wheel was used, and turned by an Arduino-controlled rotator. Powers were read by a Thorlabs power meter simultaneously by using a glass coverslip to reflect 5% of the incoming flux.

For the spectra shown in Fig. 3a, an excitation fluence of 5 Wcm^{-2} was used, and signal was collected using a Hamamatsu photomultiplier tube (PMT) with a wide spectral response (model R928). The 30% Gd^{3+} spectrum has a maximum intensity that is >4660 times larger than the measured noise floor of the detector, which is dominated by dark current. Conservatively assuming a quadratic dependence of upconverted emission on excitation fluence, this implies that signal levels larger than the noise floor are expected to be detected for excitation intensities of $(5/(4660)^{0.5})$ Wcm^{-2}; or <100 $mWcm^{-2}$.

Time-gated Triplet Phosphorescence Measurement

The triplet spectrum was measured on a modern setup modeled after the phosphorimeters of the past century, in which excitation light is blocked while emitted light from the sample is being collected, in order to only collect long-lifetime emission events (Figure

S4). A Chameleon Ti:Sapphire tunable laser from Coherent was used as the excitation source. The laser wavelength was tuned to 791 nm in the fundamental beam (2.8 mW CW power). A physical optical chopper was used at a frequency of 500 Hz to ensure the laser was completely attenuated during "off" times. The chopper was controlled by a central delay pulse generator (Quantum Composer) which was also used to modulate the avalanche photodiode (APD, Excelitas SPCM-AQRH) on and off out of phase with the chopper, with an 8-μs delay between the chopper and the APD. The sample was made akin to the encapsulation technique using $NaGdF_4$ UCNPs with no Yb^{3+} or Er^{3+} to exclude the possibility of long-lived lanthanide phosphorescence. However, after spin-coating the IR806-UCNP/ polystyrene suspension onto the Si wafer, it was not encapsulated with UV-curable polymer, but instead was attached to the cold finger of a cryogenic microscope stage (Linkam Scientific) inside the glovebox using silver paste to ensure thermal conductivity (Perkin Elmer), and cooled to 80 K using liquid N_2. Two 808 longpass filters were placed in the emission path (Semrock 808LP RazorEdge). The APD was set up behind a monochromator and the monochromator swept from 800 nm to 1020 nm. Each 0.5 nm position of the monochromator was integrated for 20 seconds. A blank sample of $NaGdF_4$ UCNPs with no dye was also measured to ensure no Yb^{3+} or Er^{3+} contribution, and was subtracted out of the peak shown in Fig 2a.

Two-photon Excitation Spectrum

To further elucidate the presence of a lower-lying triplet state, an excitation spectrum of the dye film was taken. IR806 dye was mixed with a 5 mg/mL solution of PMMA in toluene in a N_2 glovebox, and spun onto a Si wafer with a 100 nm SiO_x top layer. The wafer was quickly placed under vacuum, attached to the cold finger of a cryostat (Janis ST-500). The sample was cooled to 77 K. The same Ti: Sapphire laser as above was used, and the excitation wavelength was scanned from 910 - 1040nm. Two 850SP dichroic filters (ThorLabs) were placed in the emission path of the microscope, and a 900LP (Semrock) filter was placed in the excitation path to ensure no high-energy features of the laser could pass. An Andor iXon EMCCD camera was used to collect the spectra, with 2 second integrations and the binning set to 4. Singlet emission from 700-850nm was integrated for each excitation wavelength, and forward and back sweeps were averaged to obtain the spectrum shown below.

To obtain the power dependence of the shoulder feature, the laser wavelength was fixed near the excitation spectrum's peak at 980 nm, while the power was tuned across approximately 1.5 orders of magnitude. Each point represents a singlet emission spectrum integrated as above from 700 – 850 nm. The blue points represent both the forward and back scans. The green line has a slope equal to 1.84, clearly showing the two-photon dependence inherent with this feature.

Singlet Lifetime Measurements

Singlet lifetimes were measured using a supercontinuum laser (Leukos Rock 450 at 40 MHz) where the wavelength was tuned with an acousto-optic tunable filter (AOTF, Gooch and Housego) to 693 nm, exciting the high-energy tail of the IR806 singlet absorption feature. A 740 LP dichroic filter (ThorLabs) was placed in the emission path of the microscope to block any reflected laser light. Approximately 1 μW of laser power

was focused using a long-working-distance objective (Nikon Super Plan Fluor 40x, 0.6 NA, 2.8 mm WD) into a sealed quartz cuvette (Starna) containing the relevant dye or IR806-UCNP dispersion, sealed in an N_2 glovebox as above. Emission was collected using a single-photon avalanche photodiode (MPD PDM) with <50 ps timing resolution, connected to a time-correlated single-photon detector (Picoquant) with 4 ps resolution. Samples were diluted ~100x relative to the concentrations used in the upconverted emission measurements. Data were fitted using single exponential fits over the first 1 ns of decay. Single exponentials were used to elucidate the average decay behavior, and are unaffected by instrument response (~40 ps).

Quantum Yield Measurements

To determine the upconversion quantum yields (UCQYs), 500 μL of a UCNP dispersion in toluene was placed in a quartz cuvette with a Teflon cap, sealed with Teflon tape, and placed in an integrating sphere (Horiba Jobin-Yvon) for the Fluorolog-3 spectrometer. Unfunctionalized UCNP UCQY measurements were performed under ambient atmosphere. IR806-UCNPs were dispersed in anhydrous toluene, sealed in an N_2-glovebox and wrapped with Teflon tape before removing from the box. The light paths between the excitation laser (Sheaumann, 976 nm, 1 W for bare UCNPs, Hi-tech Optoelectronics Co., 800 nm for IR806-UCNPs), integrating sphere, and the spectrometer were routed using fiber optic bundles (Fiberoptic Systems, Inc). For each sample, the emission was measured from 510 to 680 nm. The unabsorbed laser radiation (excitation spectrum) was measured at the detector from 970 to 984 nm for bare UCNPs, or 794-804 nm for IR806-UCNPs. For IR806-UCNPs an 808 nm notch filter (Semrock) was used to attenuate the laser light so as not to saturate the detector. Pure toluene was used to record blank excitation and emission spectra. Excitation and emission spectra were corrected for the sensitivity of the detector over the appropriate wavelengths using a NIST-traceable calibrated light source (Avantes Avalight HAL-CAL) with the same integrating sphere, fiber optic setup, detector, and spectrometer settings. Excitation spectra were also corrected using the transmission spectrum of the 808 nm notch filter. Reported UCQYs are the result of five UCQY measurements for each sample that have been averaged. Occasionally, 'ripening' of the QY was observed for dye-sensitized samples, meaning recorded UCQY measurements showed an appreciable increase in QY upon successive measurements. This is attributed to both a decrease in absorption and increase in emission, the causes of which are currently unknown. Each UCQY measurement was calculated using the four intensity values as follows:

$$UCQY = (I_{em,\,sample} - I_{em,\,blank}) \div (I_{ex,\,blank} - I_{ex,\,sample})$$

where I_{em} represents the integrated emission from 510 - 680 nm, and I_{ex} represents the transmitted laser radiation, integrated from 970 - 984 nm (794 - 804 nm for dye excitation).

Any IR806 unbound to the UCNPs may reduce apparent efficiency through an inner filter effect, by absorbing incident light without transferring that energy into the nanoparticle (i.e., the real UCQYs may be larger than what we report). The absence of an unquenched component in IR806-UCNP singlet lifetime data (Fig. 3b) suggests the free dye contribution is minor, so any reductions in UCQYs are also likely to be minor.

Cyclooctatetraene Experiments

To obtain the cyclooctatetraene (COT) dependences in Fig. 3a, IR806-UCNP samples were prepared as above in a N_2 glovebox. A fresh bottle of COT (Sigma) was brought into the glovebox and stored there. The IR806-UCNP sample (or in the case of the control, UCNP sample) was diluted five-fold such that a 50uL aliquot of the same sample could be used for all COT concentrations within a single experiment. Because of photodegradation of COT, only two UCQY measurements were averaged for each sample. Toluene mixed with the appropriate amount of COT was used to record blank excitation and emission spectra.

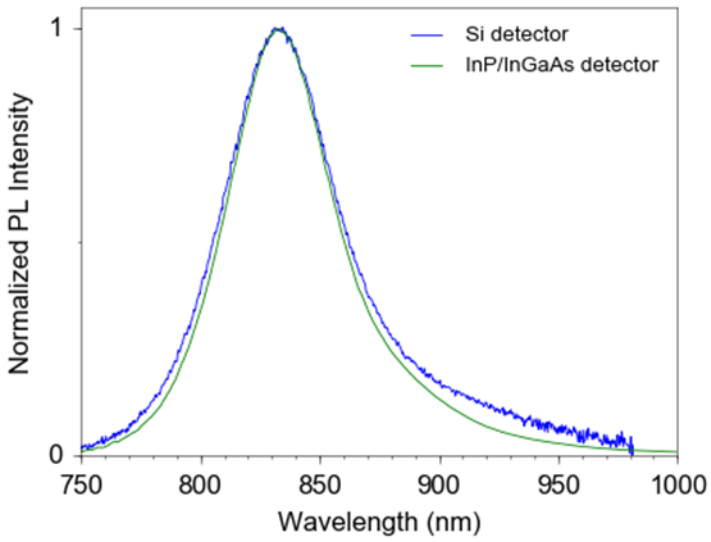

Supplementary Figure 1: Comparison of IR806 emission spectra collected with different detectors. Emission collected with a Si detector is shown in blue, while emission collected with an InP/InGaAs detector is shown in green. Details for the measurements and the two detectors are provided in the Supplemental Methods.

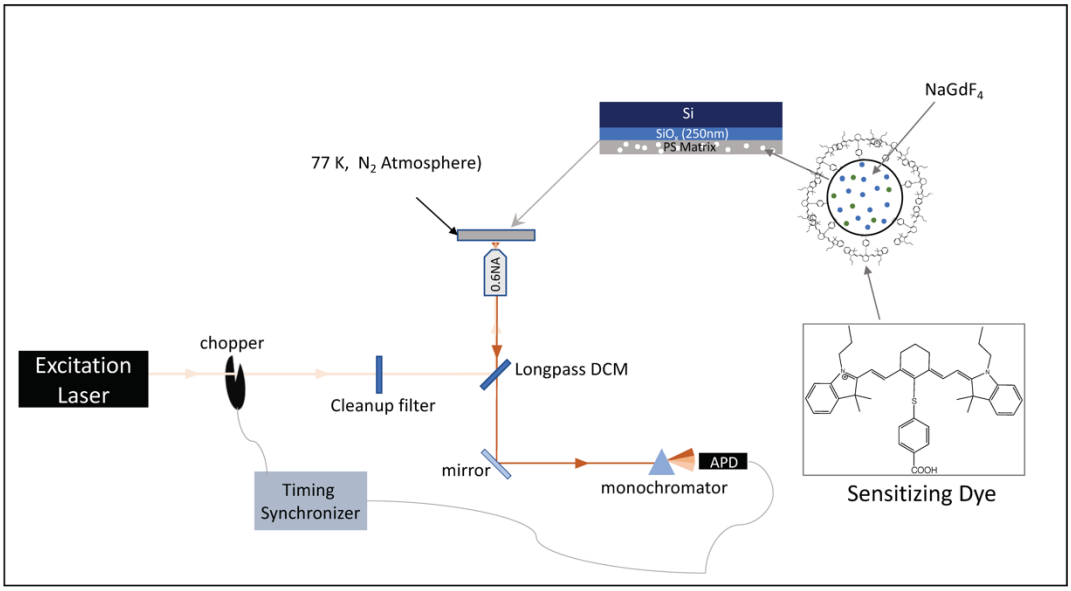

Supplementary Figure 2. Cartoon schematic of time-gated triplet phosphorescence setup.

A Chameleon Ti:Sapphire tunable laser from Coherent was used as the excitation source. The laser wavelength was tuned to 791 nm in the fundamental beam (2.8 mW CW power). A physical optical chopper was used at a frequency of 500 Hz to ensure the laser was completely attenuated during "off" times. The chopper was controlled by a central delay pulse generator (Quantum Composer) which was also used to modulate the avalanche photodiode (APD, Excelitas SPCM-AQRH) on and off out of phase with the chopper, with an 8-µs delay between the chopper and the APD. Two 808 longpass filters were placed in the emission path (Semrock 808LP RazorEdge). The APD was set up behind a monochromator and the monochromator swept from 800 nm to 1020 nm. Each 0.5 nm position of the monochromator was integrated for 20 seconds. A blank sample of $NaGdF_4$ UCNPs with no dye was also measured to ensure no Yb^{3+} or Er^{3+} contribution, and was subtracted out of the peak shown in Fig 2A. See Methods for additional details.

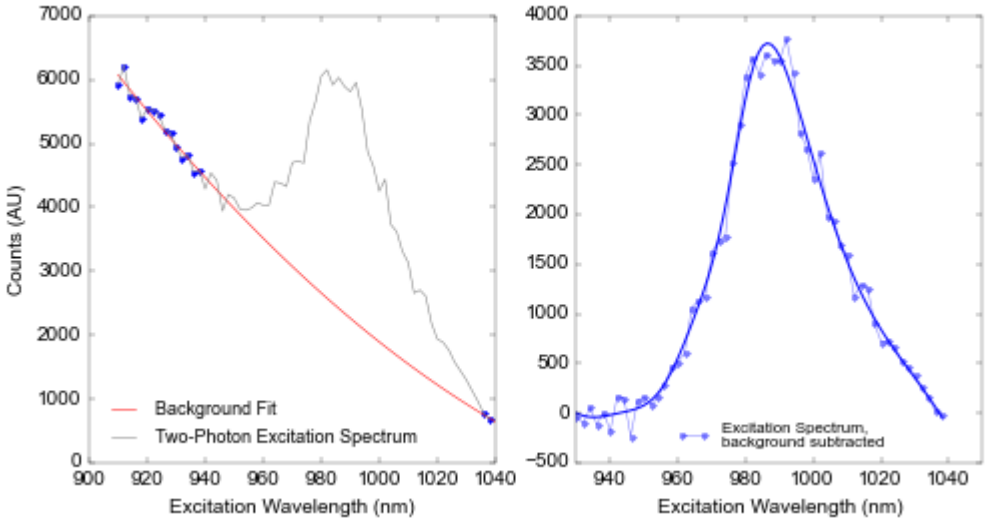

Supplementary Figure 3. IR806 two-photon excitation spectrum

(*Left*) Two-photon excitation spectrum of IR806 film under vacuum and cooled to 77K. The measurement was taken by integrating IR806 singlet emission (700 - 850 nm) while sweeping the excitation wavelength from 910 – 1040 nm. The average excitation laser power was ~10^6 W/cm^2 at all wavelengths, assuming a diffraction-limited spot, and the laser repetition rate and pulse width were ~80 MHz and 140 fs, respectively (Ti:Sapph oscillator, Coherent Inc). Blue dots represent data points used to calculate the background signal (red line), attributed to absorption through the low-energy tail vibronics of the S_1 state. The background was fitted to a double polynomial. (*Right*) Background-subtracted two-photon action spectrum of IR806 (blue dots) and smoothed curve (blue line). This resonant feature is attributed to the two-photon excitation of the singlet state via the dye T_1 state as an intermediate.

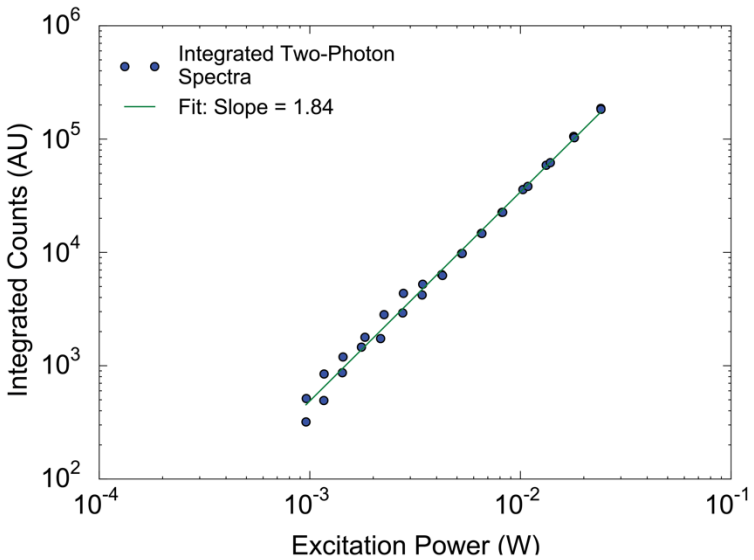

Supplementary Figure 4. IR806 two-photon action spectrum power dependence. The excitation wavelength was fixed at 980 nm, near the peak intensity of the resonance feature in Supplementary Figure 2, and the integrated emission measured from 700 – 850 nm. The laser power was varied across ~1.5 orders of magnitude. Data points are both the forward and back scans in power. Fitted green line slope is 1.84, showing the two-photon dependence inherent with this feature.

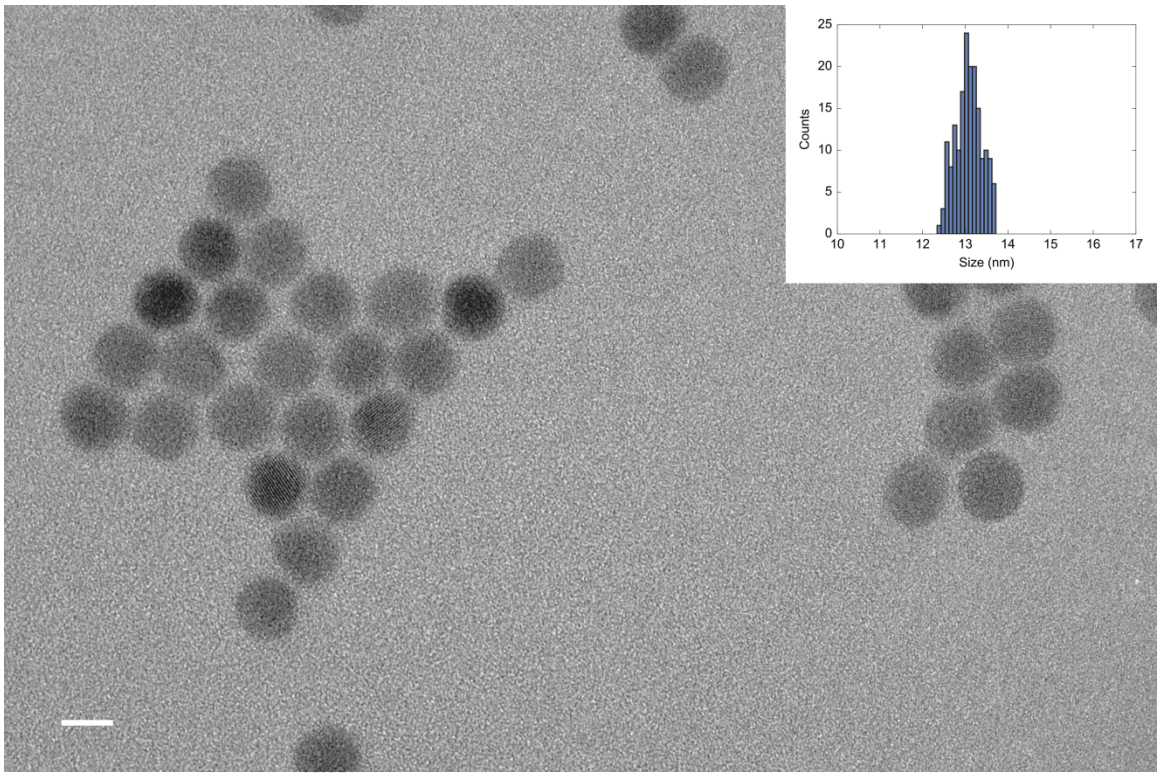

Supplementary Figure 5. Representative transmission electron micrograph of $NaY_{0.48}Gd_{0.3}Yb_{0.2}Er_{0.02}F_4$ nanocrystals.

Scale bar = 10 nm. Inset: size histogram, measured with ImageJ software from multiple High-Angle Annular Dark Field electron microscope images to improve the Z-contrast for automated sizing. Average size is 13.1 ± 1.0 nm.

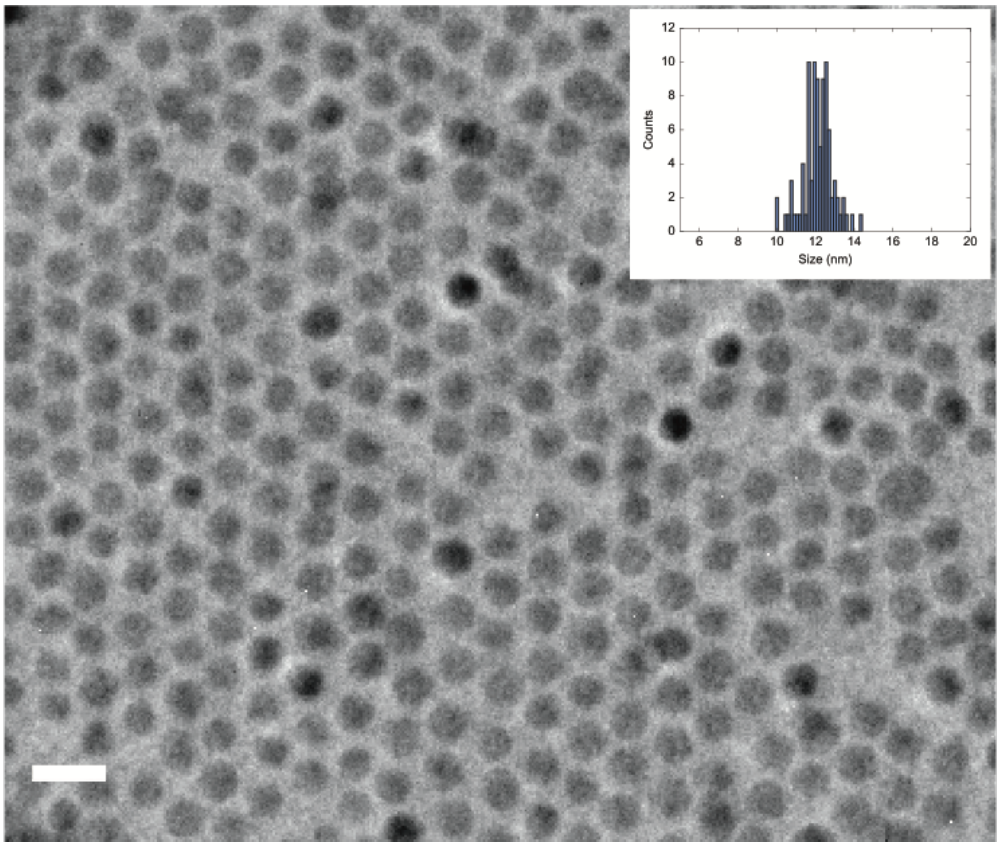

Supplementary Figure 6. Representative transmission electron micrograph of $NaY_{0.78}Yb_{0.2}Er_{0.02}F_4$ nanocrystals.

Scale bar = 20 nm. Inset: size histogram, measured with ImageJ software from multiple High-Angle Annular Dark Field electron microscope images to improve the Z-contrast for automated sizing. Average size is 12.1 ± 0.8 nm.

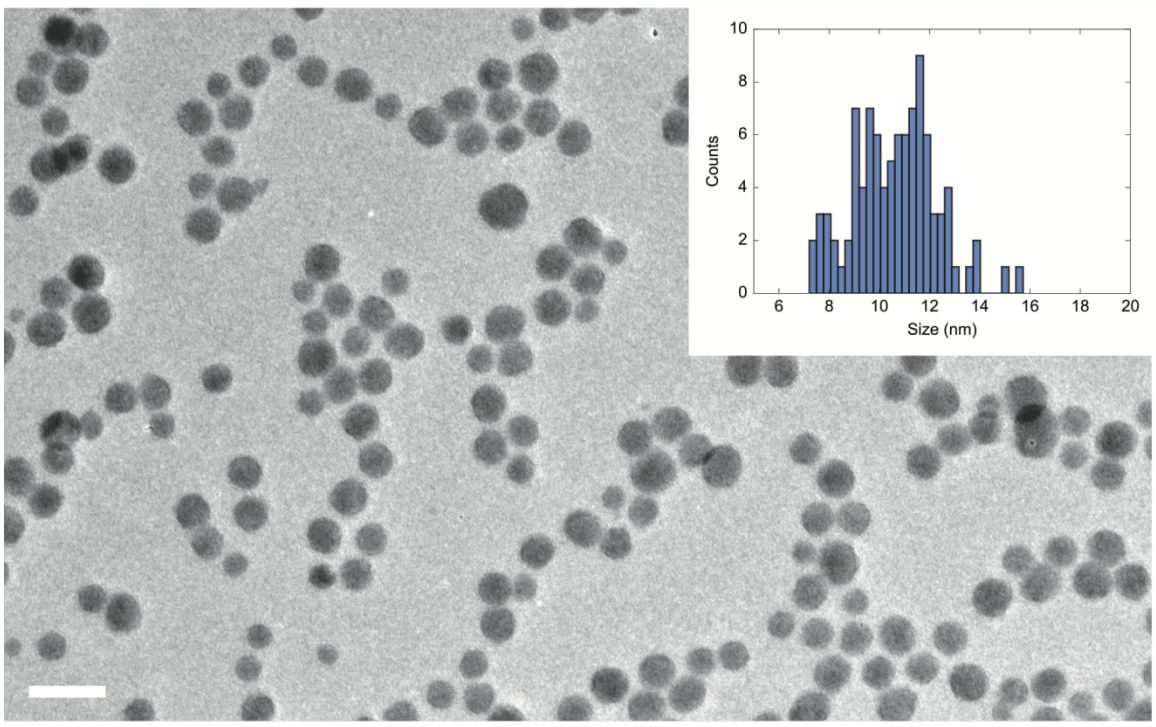

Supplementary Figure 7. Representative transmission electron micrograph of $NaGd_{0.78}Yb_{0.2}Er_{0.02}F_4$ nanocrystals.

Scale bar = 20 nm. Inset: size histogram, measured with ImageJ software from multiple High-Angle Annular Dark Field electron microscope images to improve the Z-contrast for automated sizing. Average size is 10.6 ± 1.7 nm.

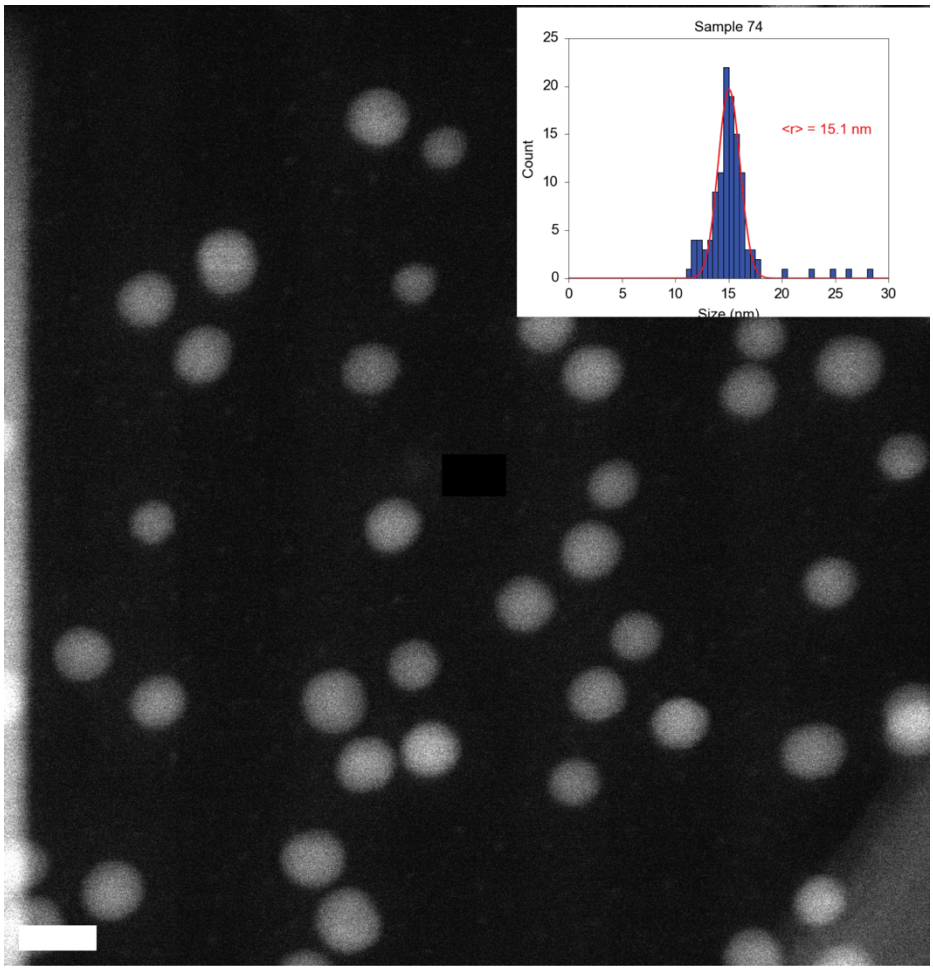

Supplementary Figure 8. Representative transmission electron micrograph of $NaGd_{0.2}Y_{0.58}Yb_{0.2}Er_{0.02}F_4$ nanocrystals.

Scale bar = 20 nm. Inset: size histogram, measured with ImageJ software from multiple High-Angle Annular Dark Field electron microscope images to improve the Z-contrast for automated sizing. Average size is 15.1 ± **1.0 nm.**

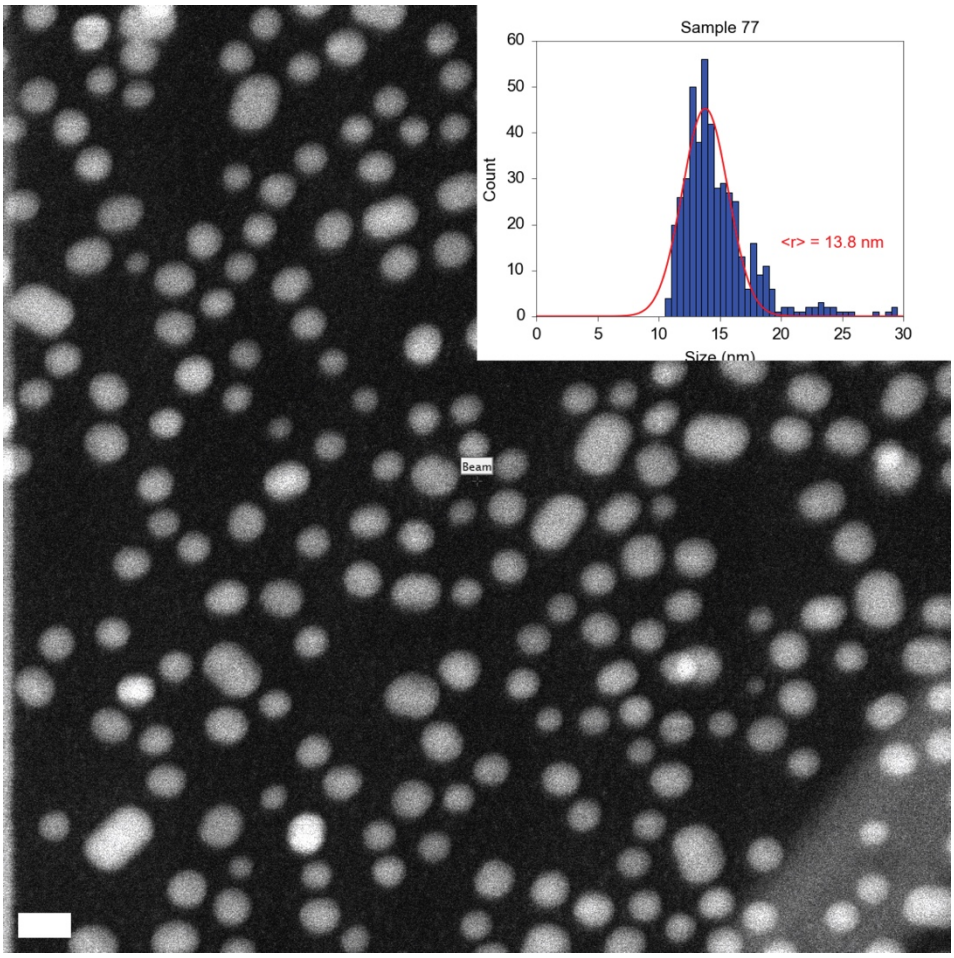

Supplementary Figure 9. Representative transmission electron micrograph of Na $Gd_{0.4}Y_{0.38}Yb_{0.2}Er_{0.02}F_4$ nanocrystals.

Scale bar = 20 nm. Inset: size histogram, measured with ImageJ software from multiple High-Angle Annular Dark Field electron microscope images to improve the Z-contrast for automated sizing. Average size is 13.8 ± **1.9 nm.**

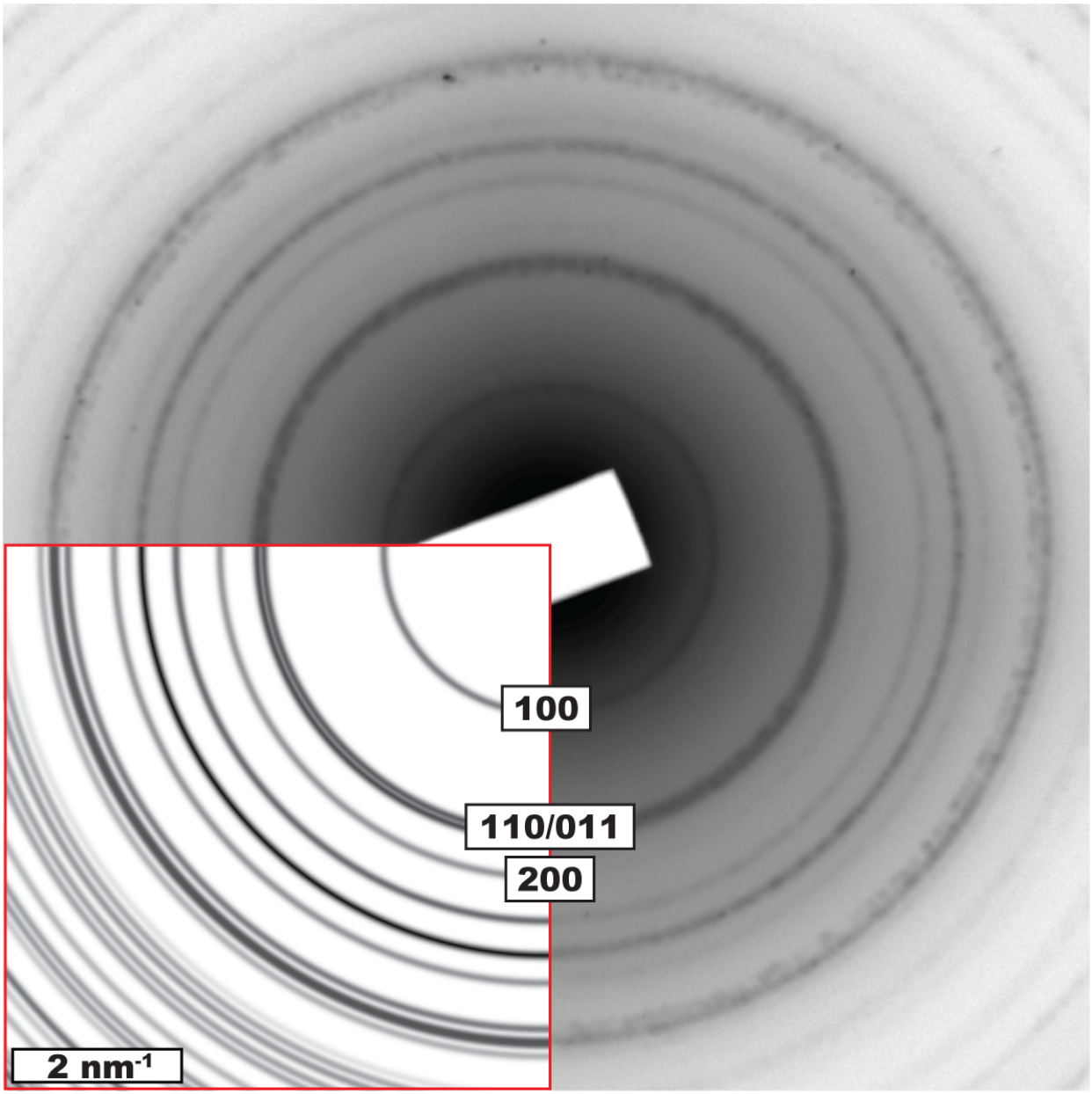

Supplementary Figure 10. Representative diffraction pattern of UCNPs

Pattern taken with a parallel electron beam of 1 μm diameter over a dense region of UCNPs. Inset shows kinematic simulation calculated with CrystalMaker software. The pattern shows 100% β-phase $NaYF_4$ crystal structure.

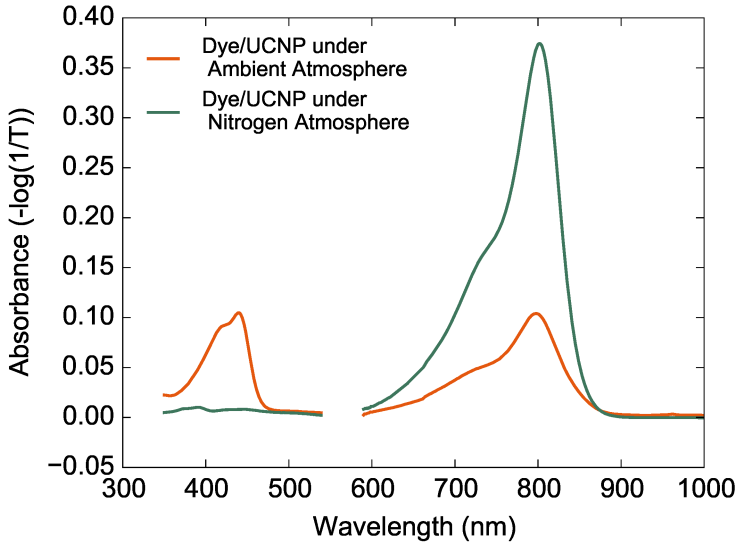

Supplementary Figure 11. IR806-UCNP steady-state stability in air

Absorbance spectra of $NaGdF_4$ nanoparticles dye functionalized in the glovebox (green line) or in air (orange line). When the functionalization was performed in air, the dye undergoes a rapid and visible color change from blue green to orange. However, when functionalized in an inert N_2 glovebox, the dye color remains stable

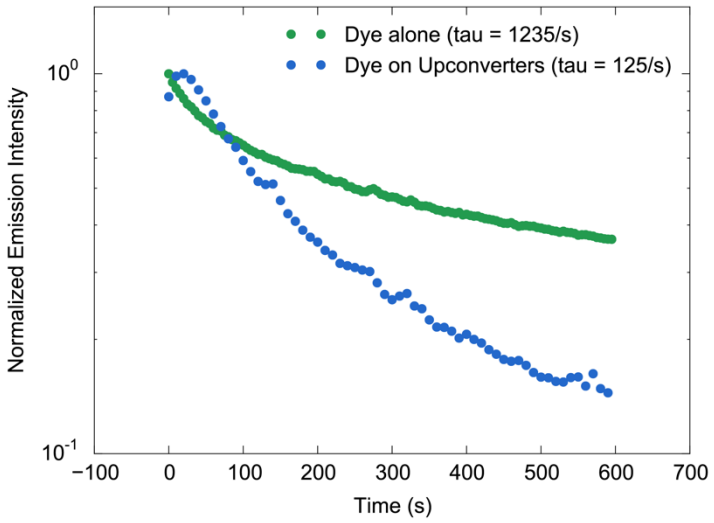

Supplementary Figure 12. IR806-UCNP dynamic stability

Films of IR806-UCNPs were made akin to the films in time-gated triplet phosphorescence measurements, but were left at room temperature instead of cooling to cryogenic temperatures. For the air studies the cryostat was opened to air. A series of emissions from a film of IR806-$NaGdF_4$ prepared in a glovebox was measured in a system analogous to upconverted emission measurements, where the spectrometer recorded one spectrum after another. Data was then condensed to a single point by integrating each emission spectrum from 500 - 700 nm. Emission from a film of the dye on and off the $NaGdF_4$ nanoparticles reveals the IR806-Gd^{3+} conjugate photobleaches an order of magnitude faster than the dye alone.

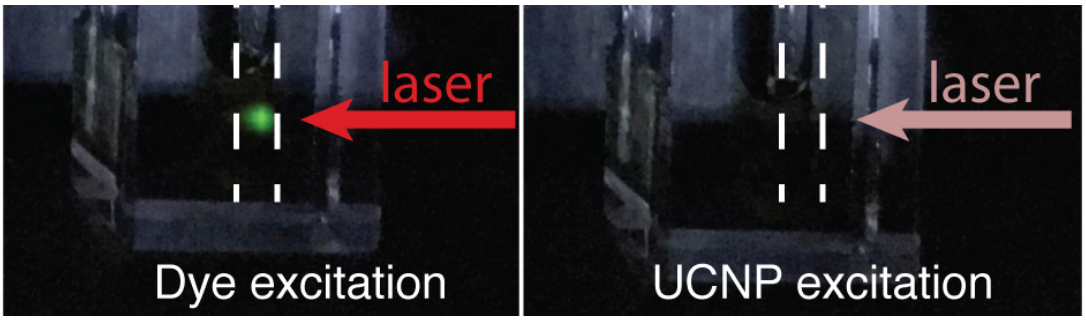

Supplementary Figure 13. Visible upconverted emission at low excitation flux. A solution of IR806-functionalized $NaY_{0.48}Gd_{0.3}Yb_{0.2}Er_{0.02}F_4$ UCNPs under N_2 atmosphere in a Starna fluorescence 18F-Q-10-GL14-C quartz cuvette (path length 2mm). The images were taken with the camera of an Apple iPhone 7—Left: excited with 1.8 Wcm^{-2} 808nm collimated laser light, and Right: excited with 1.8 Wcm^{-2} 980nm collimated laser light. As can be seen, visible upconverted emission is clearly observed when exciting the dye antennae, but not when exciting the UCNPs directly.

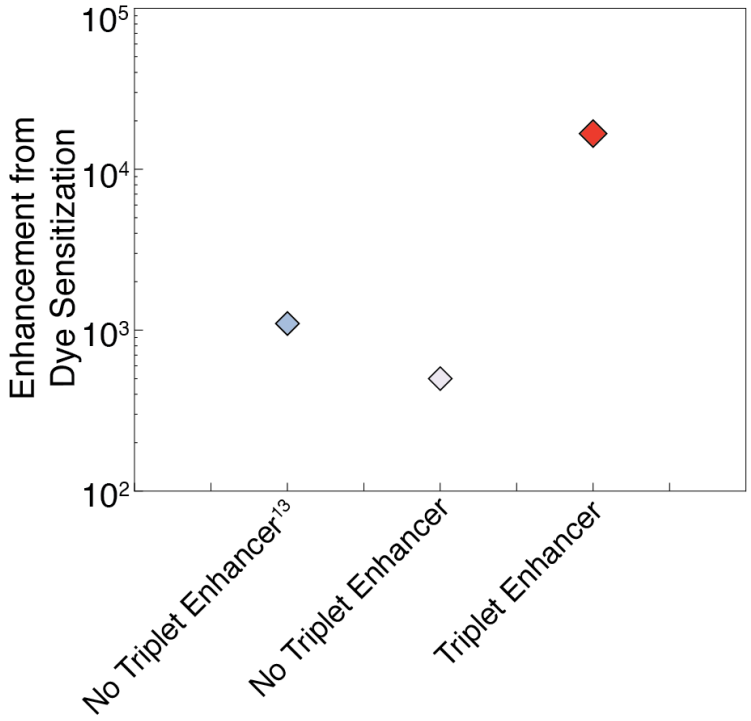

Supplementary Figure 14. Brightness enhancement from dye sensitization
Comparison of brightness enhancements from dye excitation divided by direct nanoparticle excitation: dye-sensitized β–$NaY_{0.78}Yb_{0.2}Er_{0.02}F_4$ cores (0% Gd^{3+} (Nat. Phot. 6, 560-564))[13], dye-sensitized β–$NaY_{0.78}Yb_{0.2}Er_{0.02}F_4$ cores (0% Gd^{3+}), and dye-sensitized β–$NaY_{0.78}Gd_{0.3}Yb0_{.2}Er_{0.02}F_4$ cores (30% Gd^{3+}).

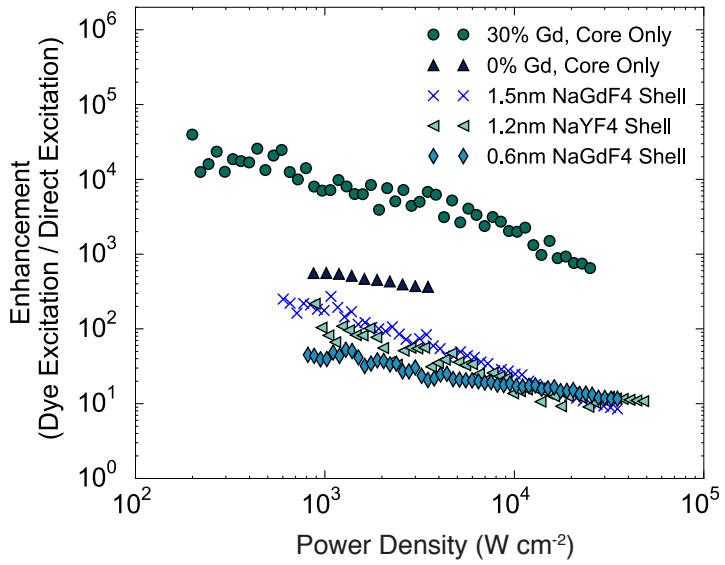

Supplementary Figure 15. Power-dependent enhancement from dye sensitization

Comparison across many UCNP systems sensitized with IR806 dye showing the relative increase in upconverted brightness from exciting the system directly with 980 nm light versus exciting the system through the dye antenna at 808 nm. The 0% Gd^{3+}, core sample is analogous to that used by Zou *et al*.[13] As can be seen, the 30% Gd^{3+} cores show remarkably high brightness enhancements. It is worth noting that the enhancement factors increase with decreasing power. Thus, while we cannot strictly measure an enhancement factor at excitation intensities in the W/cm2 range (there is no emission from the 980 nm excited particles at these fluences), we know it is >33,000.

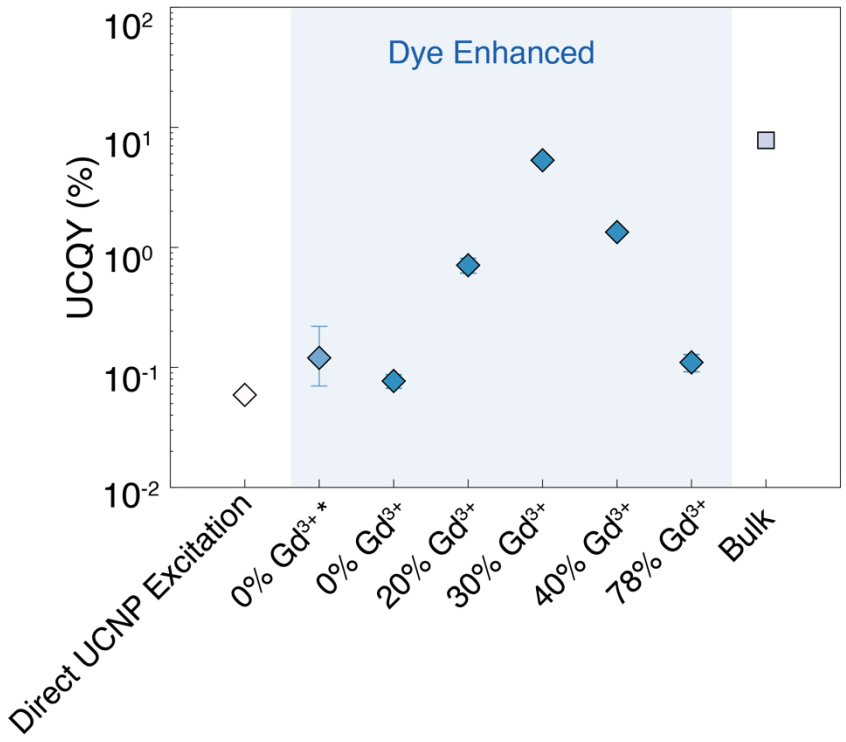

Supplementary Figure 16: Comparison of UCQYs of various UCNPs
All UCNP compositions above contain 20% Yb^{3+} and 2% Er^{3+}. Quantum yields from (left to right) directly-excited 30% Gd^{3+} cores, dye-sensitized 0% Gd^{3+} value from literature[13], dye-sensitized 0% Gd^{3+} cores, dye-sensitized 20% Gd^{3+} cores, dye-sensitized 30% Gd^{3+} cores, dye-sensitized 40% Gd^{3+} cores, dye-sensitized 78% Gd^{3+} cores, and a bulk upconverting crystal[14]. Dye-sensitized UCQYs were measured at 5 W cm^{-2} excitation intensity. As in Fig. 4b, all points contain error bars, but for most the error was smaller than the symbol itself.

Optimized DFT Geometry	XCF	TDA (eV)	no TDA (eV)
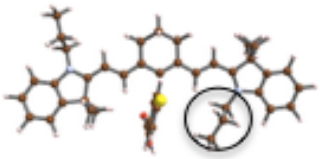	PBE0	1.0	0.8
	B3LYP	1.0	0.9
	BHLYP	1.0	0.6
	wB97X-D	1.0	0.3
	CAM-B3LYP	0.9	0.4
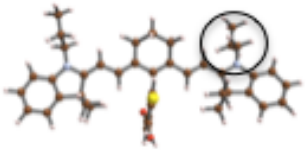	B3LYP	1.0	0.9
	BHLYP	1.2	0.8

Supplementary Table 1. Lowest lying triplet energies from TDDFT calculations. Exchange Correlation Functional (XCF), Tamm Dancoff approximation (TDA).

Supplementary Discussion

Discussion of Energy Transfer Kinetics

Comparing lifetimes of free IR806 and of IR806 on UCNPs with 0% Gd^{3+} (or, 22% total lanthanide composition) in Fig. 3b, we observe a reduction in dye lifetime by a factor of ~2 when functionalized to the 0% Gd^{3+} UCNPs (575 ps vs. 293 ps). This is consistent with similar measurements in Zou *et al*.[13]

The decay rate of the singlet excited state of the dye can be written as:

$$k_{SingletState} = k_{dye} + k_{FRET} + k_{ISC}$$

where k_{ISC} is the intersystem crossing rate from the singlet excited state S_1 to the triplet state T_1; k_{FRET} is the FRET rate from S_1 to the UCNP, and k_{dye} is the decay rate of S_1 when not in the presence of FRET acceptors or heavy atoms, which we take here to be equal to the decay rate of the free dye.

We know from our measurements with the triplet quencher (Fig. 3c) that the UC quantum yield (UCQY) changes by ~20% when the quencher is added to the dye-UCNP complexes with 0% Gd^{3+} (22% total Ln^{3+}). From the approximately linear slope of the "dye excited" curve at low intensities in Fig. 4a, we know that the IR806-UCNPs are operating near the Yb^{3+} saturation regime due to the antenna effect of the dyes. For the IR806-UCNP complexes, the total UCQY is given by:

$$UCQY = ET_{dye-UCNP} \times QY_{UCNP}$$

where $ET_{dye-UCNP}$ is the energy transfer efficiency from the dye to the UCNP, taking into account the total absorption of the dye, and QY_{UCNP} is the upconverting quantum yield of the UCNP when pumped directly (e.g., with 980 nm excitation). In the Yb^{3+} saturation regime, QY_{UCNP} remains approximately constant, and the addition of the triplet quencher COT only effects the first term on the right, $ET_{dye-UCNP}$. In that case, if one assumes most of the dye triplets transfer their energy to the UCNP, then the ~20% reduction in UCQY implies a ~20% decrease in energy transfer from the dye to the nanoparticle. Thus these data, along with the reduction in dye singlet lifetime by ~2×, allow us to calculate the total FRET and ISC rates to be ~1/(0.72 ns) and ~1/(2.87 ns), respectively. This tells us that singlet-state FRET is the primary energy-transfer mechanism for 22% Ln^{3+} UCNPs, although ISC is not negligible and is approaching the same order of magnitude as the FRET rate.

Next, we measure nearly another 2-fold reduction in lifetime when the dye is added to the surfaces of the 30% Gd^{3+} UCNPs (52% Ln^{3+}). This gives a further increase in the ISC rate k_{ISC} to 1/(0.375 ns), which is 7.7× faster than without the additional Gd^{3+}. Importantly, this implies that decay of the dye singlet state is now dominated by a combination of ISC and FRET, with the ISC rate approximately twice the FRET rate. Further, if we assume that most triplets transfer their energy to the NP, then the primary contribution of energy transfer to the nanoparticle is now from the triplet state. More specifically ~66% of energy transfer to the NP is from the triplet. Note that this agrees remarkably well with the COT triplet quencher measurement on these UCNPs, where a ~60% reduction in UCQY is observed for dyes functionalized on the 30% Gd^{3+} UCNPs (see Fig. 3c). We note that the above analysis assumes that COT quenches most of the molecular triplets. It is possible that not all triplets are quenched, but instead that the quenching rate saturates as COT reaches a certain concentration. In this case, the actual FRET contribution would be even less than the value given above.

Comparing to previous reports, this increase in ISC rate by ~8-fold is reasonable and consistent with ISC increases seen, for example, with heavy-atom-enhanced triplet formation in organic electronic polymers[15]. Furthermore, the measured ISC rate is also consistent with previous work: as expected, it is approaching the rates observed in heavy-atom-based molecular complexes, which are often in the 10^{10}-10^{14} s^{-1} range[16–18], and is faster than the FRET rate from the singlet in this system and typical ISC rates in fluorophores.

This also emphasizes that the notable increase in enhancement relative to Zou *et al*. (~30× higher at low fluences) is rooted in 2 related mechanisms: (i) The energy transfer of the molecular triplet states to the UCNP is more efficient than for singlet states, and by converting more of the photoexcited singlets to triplets, the excitation rate of the UCNP is further enhanced at the same pump intensity. Furthermore, decreasing the excited state lifetime of the singlet state permits a larger excitation rate of dyes themselves, which is important at higher excitation fluences where the excitation rate reaches the relaxation rate; and (ii) these effects can in turn increase the upconverting quantum yield of the system since UCQY is an inherently intensity-dependent value in these nonlinear systems. These two effects are multiplicative. The improvement in UCQY due to the more-efficient ET from the triplets is particularly pronounced at low excitation intensities, where the UCQYs of the unsensitized (or less-effectively

sensitized) UCNPs fall off significantly as pump intensity is reduced, whereas the better-sensitized particles still operate at relatively high UCQY even at these lower intensities, because the molecular antennas effectively put the UCNP in the near-saturation regime of Yb^{3+} (where UCQY is much less sensitive to changes in excitation intensity). This is shown directly in Fig. 4a and Supplementary Fig. 12, where the upconverted emission enhancement factors increase as excitation power densities decrease. Also, the effect of the dyes on the UCQYs of our 30% Gd^{3+} UCNPs at low power can be seen in Fig. 4b, where the UCQY was measured at a low excitation intensity of 5 Wcm^{-2}, and can also be seen in Fig. 3a, where the two spectra were collected at the same low intensity (5 Wcm^{-2}).

Supplementary References

1. Ostrowski, A. D. *et al.* Controlled synthesis and single-particle imaging of bright , sub-10 nm lanthanide-doped upconverting nanocrystals. *ACS Nano* **6,** 2686–2692 (2012).
2. Wang, F. *et al.* Simultaneous phase and size control of upconversion nanocrystals through lanthanide doping. *Nature* **463,** 1061–5 (2010).
3. Li, X. *et al.* Successive Layer-by-Layer Strategy for Multi-Shell Epitaxial Growth: Shell Thickness and Doping Position Dependence in Upconverting Optical Properties. *Chem. Mater.* **25,** 106–112 (2013).
4. Liu, D. *et al.* Three-dimensional controlled growth of monodisperse sub-50 nm heterogeneous nanocrystals. *Nat. Commun.* **7,** 1–8 (2016).
5. Fritzinger, B., Capek, R. K., Lambert, K. & Martins, C. Utilizing Self-Exchange To Address the Binding of Carboxylic Acid Ligands to CdSe Quantum Dots. *Jacs* 10195–10201 (2010).
6. Boles, M. A., Ling, D., Hyeon, T. & Talapin, D. V. The surface science of nanocrystals. *Nat. Mater.* **15,** 141–153 (2016).
7. Martin, R. L. Natural transition orbitals. *J. Chem. Phys.* **118,** 4775–4777 (2003).
8. Mewes, J. M. *et al.* Experimental benchmark data and systematic evaluation of two a posteriori, polarizable-continuum corrections for vertical excitation energies in solution. *J. Phys. Chem. A* **119,** 5446–5464 (2015).
9. You, Z. Q., Mewes, J. M., Dreuw, A. & Herbert, J. M. Comparison of the Marcus and Pekar partitions in the context of non-equilibrium, polarizable-continuum solvation models. *J. Chem. Phys.* **143,** (2015).
10. Champagne, B., Guillaume, M. & Zutterman, F. TDDFT investigation of the optical properties of cyanine dyes. *Chem. Phys. Lett.* **425,** 105–109 (2006).
11. Fabian, J. TDDFT-calculations of Vis/NIR absorbing compounds. *Dye. Pigment.* **84,** 36–53 (2010).
12. Peach, M. J. G., Williamson, M. J. & Tozer, D. J. Influence of triplet instabilities in TDDFT. *J. Chem. Theory Comput.* **7,** 3578–3585 (2011).
13. Zou, W., Visser, C., Maduro, J. a., Pshenichnikov, M. S. & Hummelen, J. C. Broadband dye-sensitized upconversion of near-infrared light. *Nat. Photonics* **6,** 560–564 (2012).
14. Pokhrel, M., Kumar, G. A. & Sardar, D. K. Highly efficient NIR to NIR and VIS upconversion in Er3+ and Yb3+ doped in M2O2S (M = Gd, La, Y). *J. Mater. Chem. A* **1,** 11595–11606 (2013).

15. Rothe, C., King, S. & Monkman, A. P. Long-range resonantly enhanced triplet formation in luminescent polymers doped with iridium complexes. *Nat. Mater.* **5,** 463–466 (2006).
16. Baryshnikov, G., Minaev, B. & Ågren, H. Theory and calculation of the phosphorescence phenomenon. *Chem. Rev.* **117,** 6500–6537 (2017).
17. Rachford, A. A., Goeb, S. & Castellano, F. N. Accessing the triplet excited state in perylenediimides. *J. Am. Chem. Soc.* **130,** 2766–2767 (2008).
18. Danilov, E. O. *et al.* Ultrafast energy migration in platinum (II) diimine complexes bearing pyrenylacetylide chromophores. *J. Phys. Chem. A* **109,** 2465–2471 (2005).